Electronic Supplementary Information (ESI)

Interface Engineering of 3D $BiVO_4$/Fe-Based Layered Double Hydroxide Core/Shell Nanostructures for Boosting Photoelectrochemical Water Oxidation

Yukun Zhu,[a,b] Jun Ren,[c] Xianfeng Yang,[d] Guojing Chang,[b] Yuyu Bu,[e] Guodong Wei,[a] Wei Han*[a] and Dongjiang Yang*[b,f]

[a]Key Laboratory of Physics and Technology for Advanced Batteries (Ministry of Education), College of Physics, Jilin University, Changchun 130012, China

[b]Collaborative Innovation Center for Marine Biomass Fibers Materials and Textiles of Shandong Province, School of Environmental Science and Engineering, Qingdao University, Qingdao 266071, China

[c]School of Chemical and Environmental Engineering, North University of China, Taiyuan 030051, China

[d]Analytical and Testing Centre, South China University of Technology, Guangzhou 510640, China

[e]Institute of Technology and Science, Tokushima University, 2-1 Minami-Josanjima, Tokushima 770-8506, Japan

[f]Key Laboratory of Coal Science and Technology, Taiyuan University of Technology, Ministry of Education and Shanxi Province, Taiyuan 030024, China.

Email: d.yang@qdu.edu.cn (Dongjiang Yang*); whan@jlu.edu.cn (Wei Han*)

The Fabrication of $BiVO_4$ Seed Layer

For the fabrication of $BiVO_4$ seed layer on the fluorine doped tin oxide (FTO) coated glass substrate (<15 ohm·sq^{-1}, 1.5 cm ×1.5 cm),[1] $Bi(NO_3)_3 \cdot 5H_2O$ (5 mmol), NH_4VO_3 (5 mmol), and citric acid (10 mmol) were dissolved in 15 mL of 20% HNO_3 aqueous solution and stirred for 30 min to get a transparent blue colored solution. Then, 3.75 mL acetic acid and 0.6 g polyvinyl alcohol (PVA-124, Mw~195,000) were added to the above solution and stirred vigorously until the solution became transparent. 40 μL of above solution was dropped and spin-coated twice on a pre-cleaned FTO substrate at the rotation rate of 4000 rpm for 50 s, and followed by calcined in a muffle furnace at 400 °C for 3 h.

The Formation of Fe-Based Layered Double Hydroxides (LDH)

The electrochemical reaction was controlled at -1.0 V *vs.* SCE, mainly involving in the reduction of sulfate ions (SO_4^{2-}) and nitrate ions (NO_3^-) at the $BiVO_4$ film surface to generate the hydroxide ions (OH^-) and increase the pH value. Subsequently, the Ni^{2+} and Fe^{2+} ions and electro-generated OH^- can easily lead to the precipitation of bimetallic hydroxide on the surface of the film.[2,3] After the exposure in air, Fe^{2+} was converted to Fe^{3+} by the self-oxidation, leading to the fabrication of $Ni_{1-x}Fe_x$-LDH.

$$SO_4^{2-} + H_2O + 2e^- \rightarrow SO_3^{2-} + 2OH^-$$

$$NO_3^- + 7H_2O + 8e^- \rightarrow NH_4^+ + 10OH^-$$

$$(1-x)Ni^{2+} + xFe^{2+} + 2OH^- \rightarrow Ni_{1-x}^{2+}Fe_x^{2+} - OH_2$$

$$Ni_{1-x}^{2+}Fe_x^{2+} - OH_2 - xe^- \rightarrow Ni_{1-x}^{2+}Fe_x^{3+} - LDH$$

The $Co_{1-x}Fe_x$-LDH arrays were prepared *via* the same method by replacing $Ni(NO_3)_2 \cdot 6H_2O$ with $Co(NO_3)_2 \cdot 6H_2O$

Computational Models.

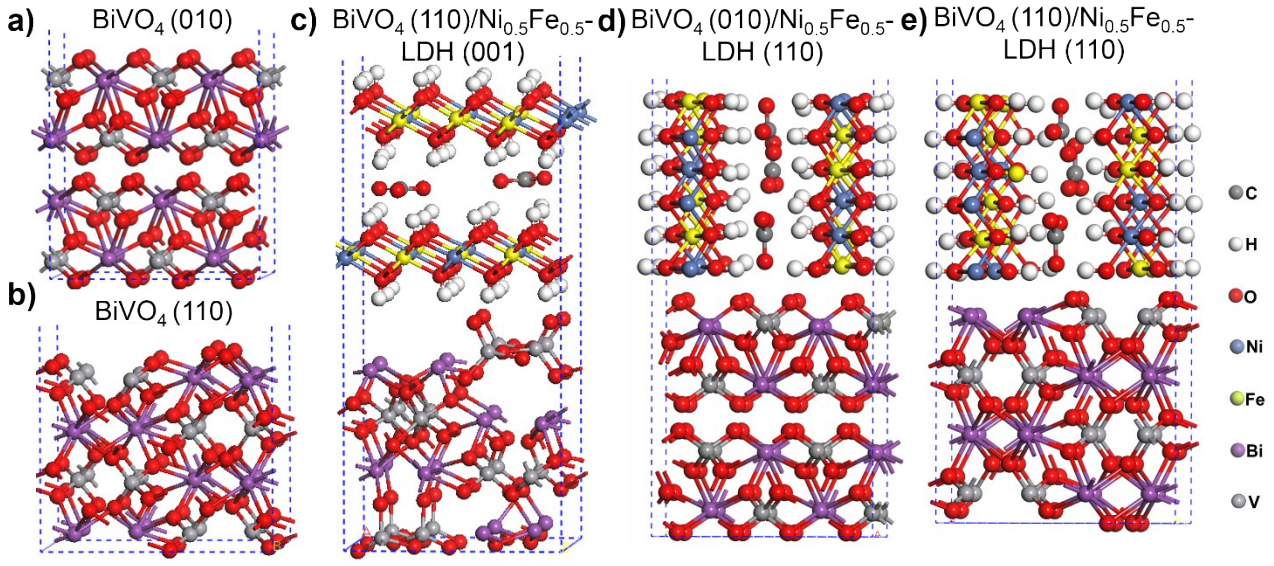

Scheme S1. The theoretical models used in the calculations. (a) $BiVO_4$ (010) surface, (b) $BiVO_4$ (110) surface, (c) $BiVO_4$ (110)/$Ni_{0.5}Fe_{0.5}$-LDH (001), (d) $BiVO_4$ (010)/$Ni_{0.5}Fe_{0.5}$-LDH (110) and (e) $BiVO_4$ (110)/$Ni_{0.5}Fe_{0.5}$-LDH (110) surface interface.

The Theoretical Calculations of Oxygen Evolution Reaction (OER).

The water splitting reaction can be written as the Equation: $2\,H_2O\,(l) \rightarrow O_2\,(g) + 2\,H_2\,(g)$. We assume that the OER is processed in the four electrons pathway, as follows:

$$H_2O\,(l) + * \rightarrow *OH + e^- + H^+$$

$$*OH \rightarrow *O + H^+ + e^-$$

$$*O + H_2O\,(l) \rightarrow *OOH + H^+ + e^-$$

$$*OOH \rightarrow O_2\,(g) + H^+ + e^-$$

The elementary steps by which the OER occurred at neutral pH are believed to involve in the adsorbed OH and O species on the surface (*) according to the following Equation:[4,5]

$$\Delta G = \Delta E + \Delta ZPE - T\Delta S + \Delta G_U + \Delta G_{PH}$$

Where the ΔE, ΔZPE and ΔS represent the different intermediates energy, zero-point energy changes, and entropy of the reaction, respectively. The ΔE is obtained from DFT calculation, while the ΔZPE and ΔS are calculated from the values in previous reports.[6] The each step of ΔG are obtained according to the approach by Rossmeisl et al.[7] The Gibbs free energies of above equation depend on the intermediates adsorption energies of *O, *OH and *OOH. They are calculated relative to H_2O and H_2 in the gas phase at U = 0.0 V, standard conditions (1.23 V *vs.* RHE), and a fixed "standard" coverage of half of the adsorbate species. U is the potential measured against RHE at standard conditions (T = 298.15 K, P = 1 bar, pH = 0). The theoretical overpotential is defined as: overpotential = max $[\Delta G_1, \Delta G_2, \Delta G_3, \Delta G_4]/e - 1.23$ V.

Supporting Figures and Discussion

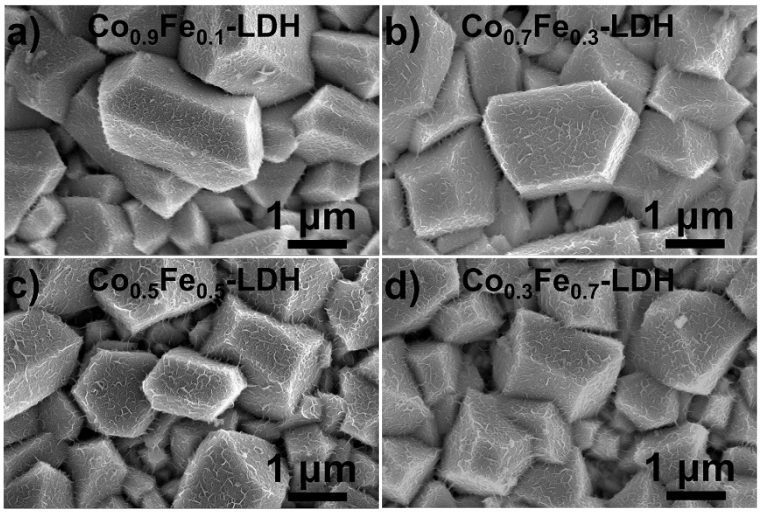

Figure S1. FESEM images of $BiVO_4/Co_{1-x}Fe_x$-LDH films.

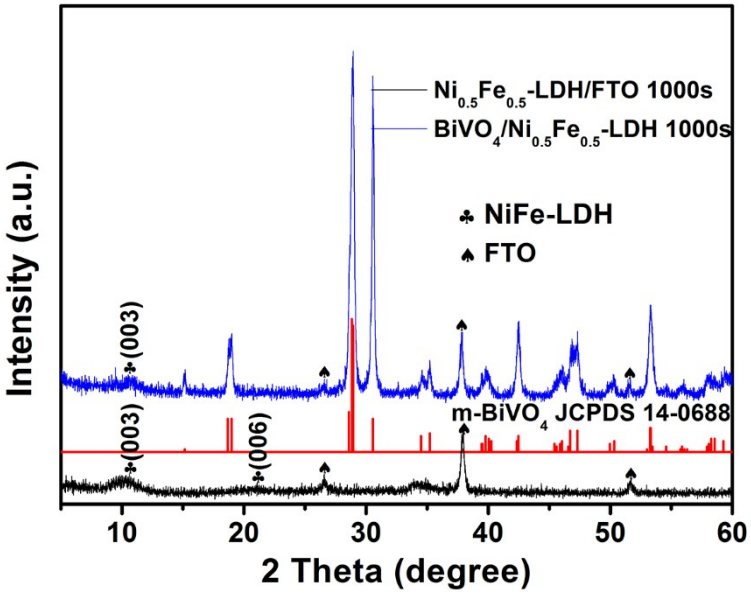

Figure S2. XRD patterns of $Ni_{0.5}Fe_{0.5}$-LDH film on FTO and $BiVO_4/Ni_{0.5}Fe_{0.5}$-LDH film that the electrodeposition time for $Ni_{0.5}Fe_{0.5}$-LDH was 1,000 s.

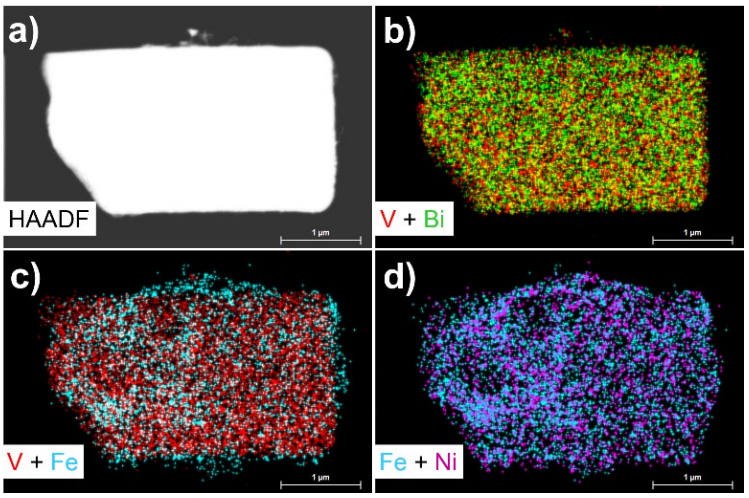

Figures S3. High Angle Annular Dark Field (HAADF)-STEM image and corresponding EDS mapping images of $BiVO_4/Ni_{0.5}Fe_{0.5}$-LDH.

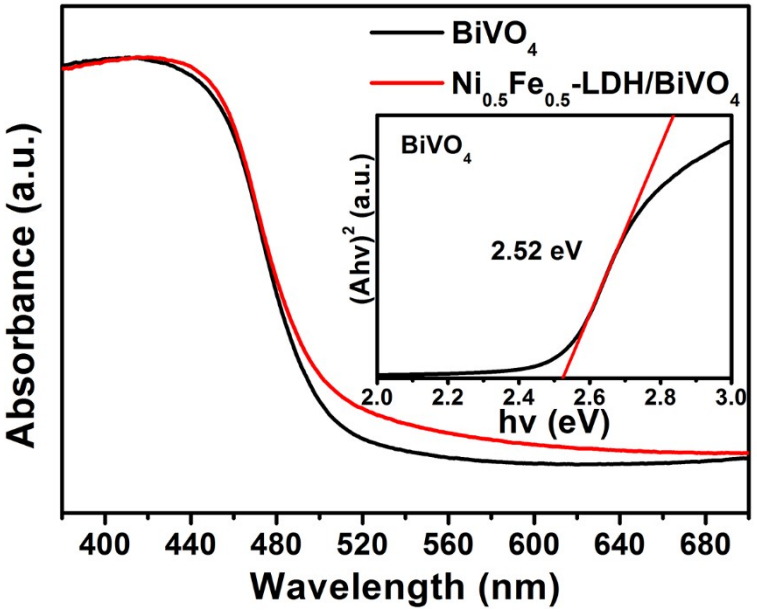

Figure S4. UV-vis absorbance spectra of the $BiVO_4$ and $BiVO_4/Ni_{0.5}Fe_{0.5}$-LDH film.

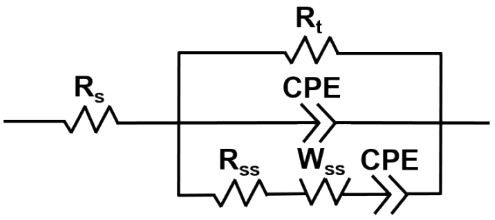

Figure S5. The equivalent circuit for fitting the EIS results. In the equivalent circuit, R_s is the solution resistance, R_t is the electron transfer resistance at the photoanode; CPE was constant phase angle element. The parallel disposition of the R_t-CPE circuit with (R_{ss}, CPE2 and W_{ss}) means the band bending in the charge space layer of the photoelectrode and surface state filling occur simultaneously when the potential changes. R_{ss}, CPE2 and W_{ss} were used to describe the behaviors of the photogenerated electron-hole pairs on the interface between the photoanode and the electrolyte. R_{ss} and W_{ss} were the electron transfer resistance at the photoanode/electrolyte interface and the Warburg resistance caused by some delay in the surface states response, respectively.[8,9]

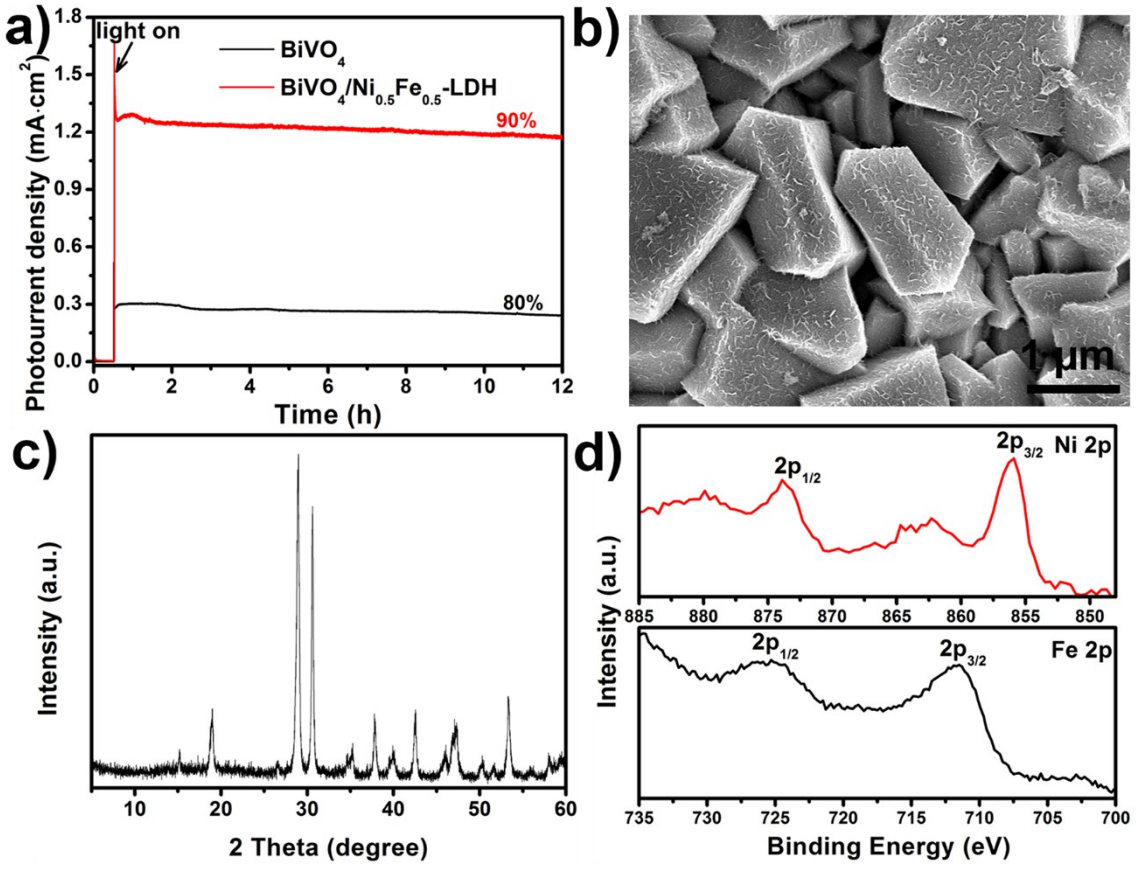

Figures S6. (a) Stability for $BiVO_4$ and $BiVO_4/Ni_{0.5}Fe_{0.5}$-LDH photoanodes under continuous illumination at 1.23 V *vs.* RHE for 12 h. (b) SEM image, (c) XRD pattern and (d) high resolution XPS spectra of Ni 2p and Fe 2p for the $BiVO_4/Ni_{0.5}Fe_{0.5}$-LDH film after continuous illumination at 1.23 V *vs.* RHE for 12 h.

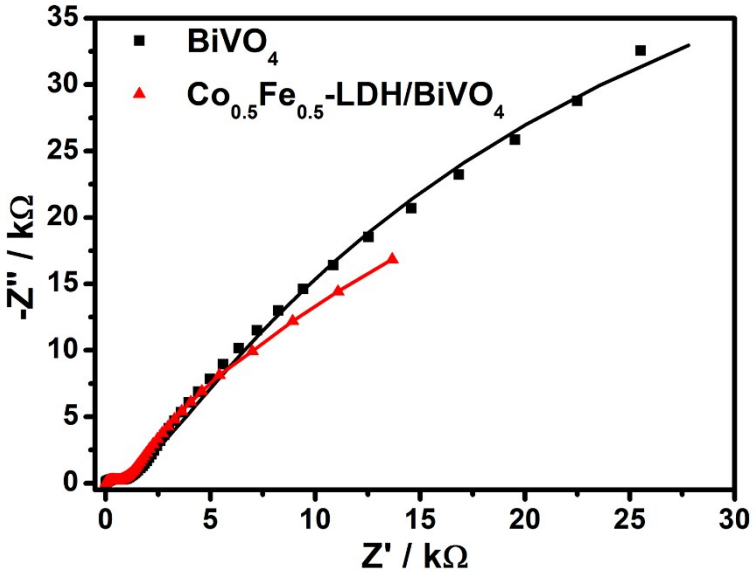

Figures S7. Nyquist plots of the EIS measured at the open circuit potential for the $BiVO_4$ and $BiVO_4/Co_{0.5}Fe_{0.5}$-LDH photoanodes under AM 1.5G (100 mW/cm^2) illumination.

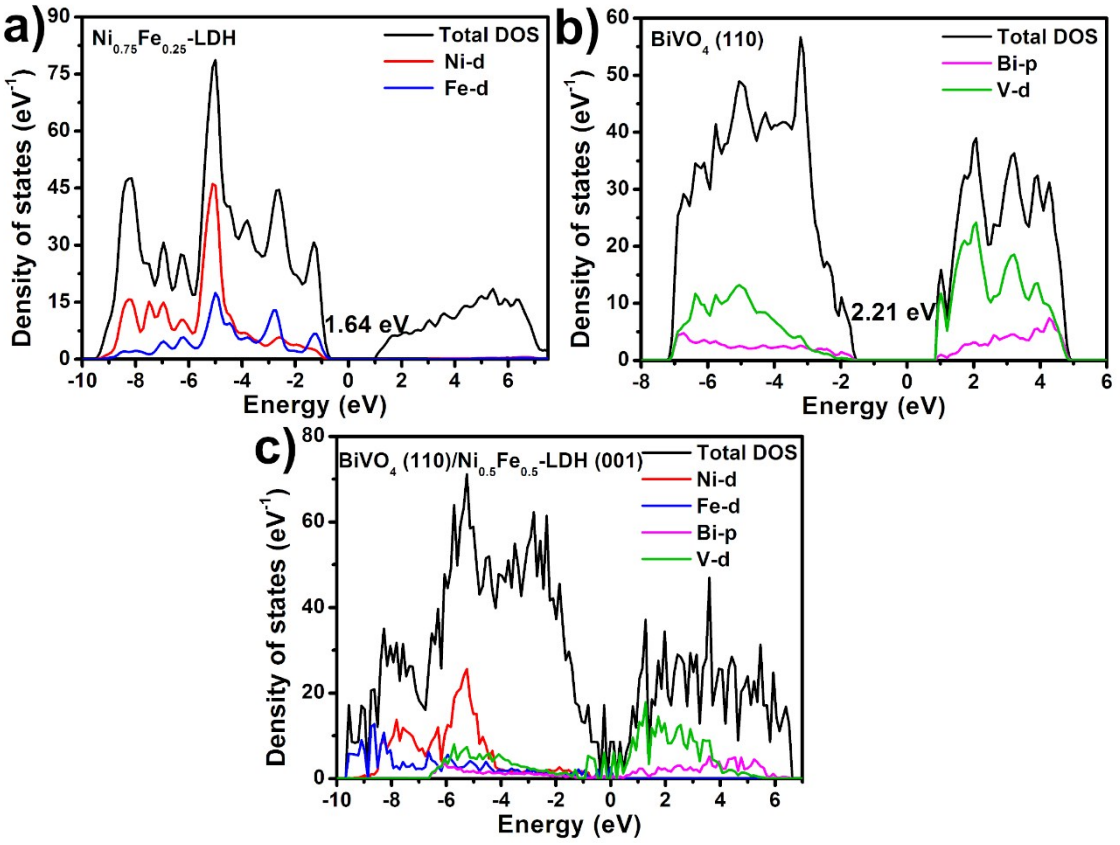

Figure S8. The density of states (DOS) of (a) $Ni_{0.75}Fe_{0.25}$-LDH surface model, (b) $BiVO_4$ (110) surface model, and (c) $BiVO_4$ (110)/$Ni_{0.5}Fe_{0.5}$-LDH interface model.

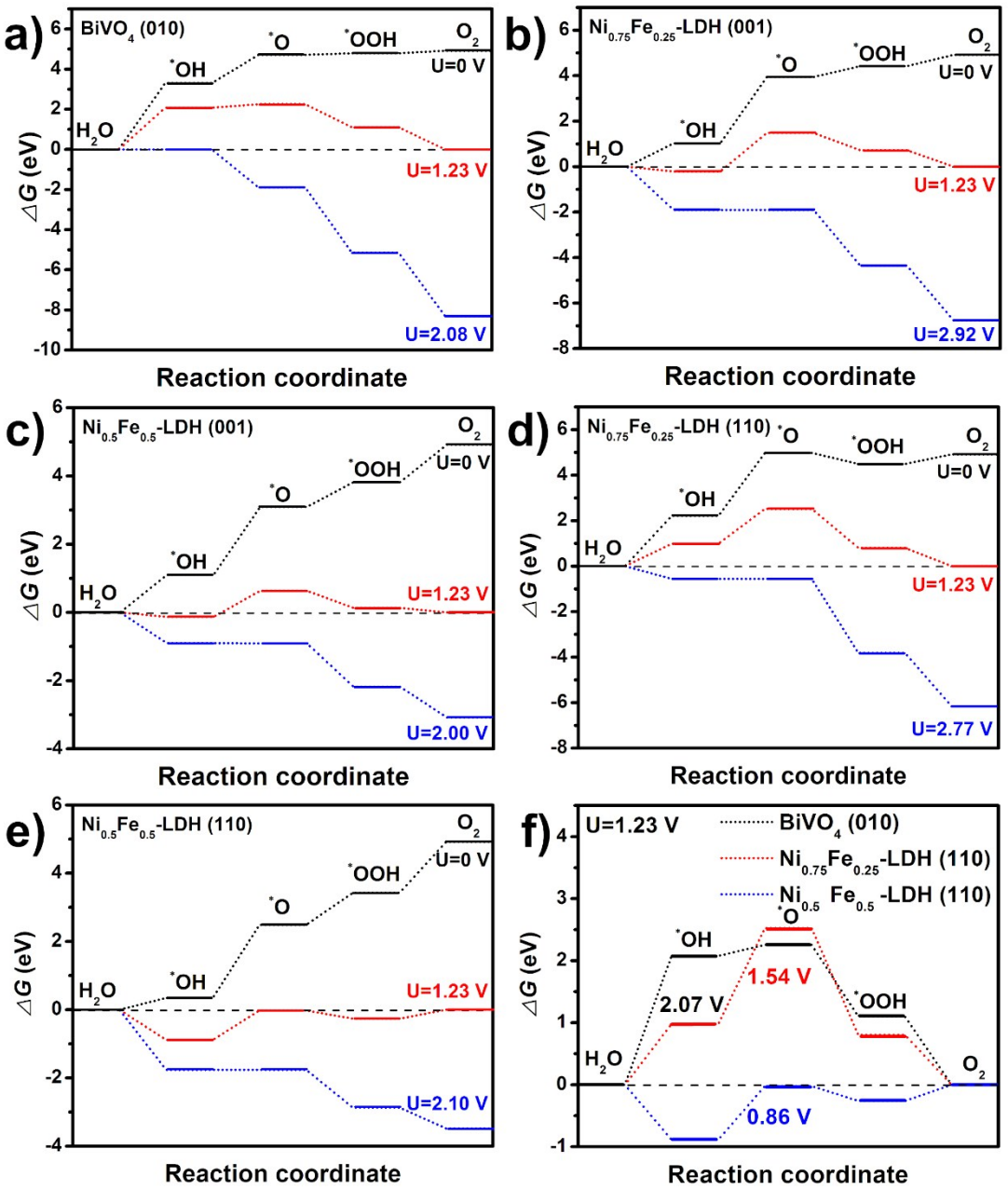

Figure S9. Standard Gibbs free energy diagrams for OER over (a) $BiVO_4$ (010) surface, (b) $Ni_{0.75}Fe_{0.25}$-LDH (001) surface, (c) $Ni_{0.5}Fe_{0.5}$-LDH (001) surface, (d) $Ni_{0.75}Fe_{0.25}$-LDH (110) surface and (e) $Ni_{0.5}Fe_{0.5}$-LDH (110) surface. (f) The OER at U=1.23 V over LDH (110) surface. The rate-determining steps for $BiVO_4$ and NiFe-LDH are the oxidation of H_2O to *OH and *OH to *O, respectively. Therefore, the overpotentials for $BiVO_4$ and NiFe-LDH are calculated from ΔG_1 and ΔG_2, respectively.

Table S1. Comparison table for the LDH/photoelectrode composites for PEC water oxidation under AM 1.5G (100 mW·cm^{-2}) illumination.

Composites	Deposition method	Deposition time	ΔE_{onset}[1] (mV)	Enhancement factor[2]	Reference
ZnO@CoNi-LDH	electrodeposition	100 s	150	3.0	10
NiFe-LDH/Ta_3N_5	solvothermal	17 h	100	2.0	11
α-Fe_2O_3/Zn-Co LDH	electrodeposition	60 s	-	1.4	12
Mn:Fe_2O_3/NiFe-LDH	hydrothermal	6 h	200	1.3	13
TiO_2/rGO/NiFe-LDH	electrodeposition	50 s	-	1.3	14
TiO_2@CoNi-LDHs	electrodeposition	30 s	-	3.3	15
TiO_2/ZnFe-LDH	photo-assisted electrodeposition	50 s	-	1.9	16
WO_3@NiFe-LDH	electrodeposition	200 s	60	1.4	17
CoAl-LDH@$BiVO_4$	hydrothermal	4 h	540	2.0	18
$BiVO_4$/CoLa-LDH	electrodeposition	20 s	530	2.0	19
CdTe@LDH@$BiVO_4$	hydrothermal	15 h	-	1.1	20
$BiVO_4$/NiFe-LDH	electrodeposition	20 s	320	4.0	This work

1. Cathodic shift of the onset potential (E_{onset}) of water oxidation photocurrent after the LDH deposition.
2. Increase of water oxidation photocurrent at 1.23 V vs. RHE after the LDH deposition.

Table S2. Fitted parameters of the EIS plots of $BiVO_4$, $BiVO_4$/$Ni_{0.5}Fe_{0.5}$-LDH and $BiVO_4$/$Co_{0.5}Fe_{0.5}$-LDH interface nanostructure photoanodes in 0.5 M Na_2SO_4 solution.

Sample	R_s (Ω·cm^2)	R_t (Ω·cm^2)	R_{ss} (kΩ·cm^2)
$BiVO_4$	13.66	690.3	108.2
$BiVO_4$/$Ni_{0.5}Fe_{0.5}$-LDH	13.31	571.2	40.87
$BiVO_4$/$Co_{0.5}Fe_{0.5}$-LDH	13.50	610.5	58.46

References

(1) Kim, C. W.; Son, Y. S.; Kang, M. J.; Kim, D. Y.; Kang, Y. S. *Adv. Energy Mater.,* 2015, 1501754.

(2) Li, Y.; Zhang, L.; Xiang, X.; Yan, D. P.; Li, F. *J. Mater. Chem. A,* 2014, **2**, 13250-13258.

(3) Lu, X. Y.; Zhao, C. *Nat. Commun.,* 2015, **6**, 6616.

(4) García-Mota, M.; Vojvodic, A.; Metiu, H.; Man, I. C.; Su, H. Y.; Rossmeisl, J.; Nørskov, J. K. *ChemCatChem,* 2011, **3**, 1607-1611.

(5) Bajdich, M.; García-Mota, M.; Vojvodic, A.; Nørskov, J. K.; Bell, A. T. *J. Am. Chem. Soc.,* 2013, **135**, 13521-13530.

(6) Valdés, Á.; Qu, Z. W. Kroes, G. J.; Rossmeisl, J.; Nørskov, J. K. *J. Phys. Chem. C,* 2008, **112**, 9872-9879.

(7) Man, I. C.; Su, H. Y.; Calle-Vallejo, F.; Hansen, H. A.; Martínez, J. I.; Inoglu, N. G.; Kitchin, J.; Jaramillo, T. F.; Nørskov, J. K.; Rossmeisl, J. *ChemCatChem,* 2011, **3**, 1159-1165.

(8) Bu, Y. Y.; Chen, Z. Y.; Li, W. B. *Appl. Catal. B: Environ.,* 2014, **144**, 622-630.

(9) Spagnol, V.; Sutter, E.; Debiemme-Chouvy, C.; Cachet, H.; Baroux, B. *Electrochim. Acta,* 2009, **54**, 1228-1232.

(10) Shao, M. F.; Ning, F. Y.; Wei, M.; Evans, D. G.; Duan, X. *Adv. Funct. Mater.*, 2014, **24**, 580-586.

(11) Wang, L.; Dionigi, F.; Nguyen, N. T.; Kirchgeorg, R.; Gliech, M.; Grigorescu, S.; Strasser, P.; Schmuki, P. *Chem. Mater.*, 2015, **27**, 2360-2366.

(12) Xu, D. Y.; Rui, Y. C.; Li, Y. G.; Zhang, Q. H.; Wang, H. Z. *Appl. Sur. Sci.*, 2015, **358**, 436-442.

(13) Huang, J. W.; Hu, G. W.; Ding, Y.; Pang, M. C.; Ma, B. C. *J. Catal.*, 2016, **340**, 261-269.

(14) Ning, F. Y.; Shao, M. F.; Xu, S. M.; Fu, Y.; Zhang, R. K.; Wei, M.; Evans, D. G.; Duan, X. *Energy Environ. Sci.*, 2016, **9**, 2633-2643.

(15) Chen, W. J.; Wang, T. T.; Xue, J. W.; Li, S. K.; Wang, Z. D.; Sun, S. *Small*, 2017, 1602420.

(16) Zhang, R. K.; Shao, M. F.; Xu, S. M.; Ning, F. Y.; Zhou, L.; Wei, M. *Nano Energy*, 2017, **33**, 21-28.

(17) Fan, X. L.; Gao, B.; Wang, T.; Huang, X. L.; Gong, H.; Xue, H. R.; Guo, H.; Song, L.; Xia, W.; He, J. P. *Appl. Catal. A*, 2016, **528**, 52-58.

(18) He, W. H.; Wang, R. R.; Zhang, L.; Zhu, J.; Xiang, X.; Li, F. *J. Mater. Chem. A*, 2015, **3**, 17977-17982.

(19) Chhetri, M.; Dey, S.; Rao, C. N. R. *ACS Energy Lett.*, 2017, **2**, 1062-1069.

(20) Tang, Y. Q.; Wang, R. R.; Yang, Y.; Yan, D. P.; Xiang, X. *ACS Appl. Mater. Interfaces*, 2016, **8**, 19446-19455